# Predicting future learning from baseline network architecture

Marcelo G. Mattar[1], Nicholas F. Wymbs[4], Andrew S. Bock[2], Geoffrey K. Aguirre[2], Scott T. Grafton[5] and Danielle S. Bassett*[3,6]

[1]Department of Psychology, University of Pennsylvania, Philadelphia, PA 19104, USA

[2]Department of Neurology, University of Pennsylvania, Philadelphia, PA 19104, USA

[3]Department of Bioengineering, University of Pennsylvania, Philadelphia, PA 19104, USA

[4]Human Brain Physiology and Stimulation Laboratory, Department of Physical Medicine and Rehabilitation, Johns Hopkins Medical Institution, Baltimore, MD, USA

[5]Department of Psychological and Brain Sciences and UCSB Brain Imaging Center, University of California, Santa Barbara, Santa Barbara, CA, USA

[6]Department of Electrical & Systems Engineering, University of Pennsylvania, Philadelphia, PA 19104, USA

*Corresponding author: dsb@seas.upenn.edu

# Abstract

Human behavior and cognition result from a complex pattern of interactions between brain regions. The flexible reconfiguration of these patterns enables behavioral adaptation, such as the acquisition of a new motor skill. Yet, the degree to which these reconfigurations depend on the brain's baseline sensorimotor integration is far from understood. Here, we asked whether spontaneous fluctuations in sensorimotor networks at baseline were predictive of individual differences in future learning. We collected functional MRI data from 22 participants prior to six weeks of training on a new motor skill. We found that visual-motor connectivity was inversely related to learning rate: sensorimotor autonomy at baseline corresponded to faster learning in the future. Using three additional scans, we found that visual-motor connectivity at baseline is a relatively stable individual trait. These results demonstrate that individual differences in motor skill learning can be reliably predicted from sensorimotor autonomy at baseline prior to task execution.

# Introduction

Adaptive biological systems display a common architectural feature that facilitates evolvability [1, 2, 3]. That feature is modularity, or near-decomposability [4], in which the system is composed of small subsystems (or modules) that each perform near-unique functions. This compartmentalization reduces the constraints on any single module, enabling it to adapt to evolving external demands relatively independently [2, 5, 6]. These principles relating modularity to adaptivity are evident across the animal kingdom, offering insights into phenomena as diverse as the developmental program of beak morphology in Darwin's finches [7] and the heterochrony of the skeletal components of the mammalian skull [8].

While an intuitive concept in organismal evolution, where genetic programs drive dynamics over long time scales, it is less clear how modularity might confer functional adaptability in neural systems whose computations are inherently transient and fleeting. To gain conceptual clarity, we consider synchronization: a foundational neural computation that facilitates communication across distributed neural units [9, 10]. Recent evidence from the field of statistical physics demonstrates that synchronization of a dynamical system is directly dependent on the heterogeneity of the associations between units [11]. Specifically, in systems where units with oscillatory dynamics are coupled in local modules, each module can synchronize separately [12], offering the potential for unique functionality and independent adaptability. These theoretical observations become intuitive when we consider *graphs*: visual representations composed of nodes that represent oscillators and edges that represent coupling between oscillators (Fig. 1a). Modules that are densely interconnected will tend to become synchronized with one another, and each module will therefore be unable to adapt its dynamics separately from the other module [12]. This highly constrained state decreases the potential for adaptability to incoming stimuli in a changing environment. Conversely, modules that are sparsely interconnected with one another will maintain the potential for adaptive, near-independent dynamics.

Given these theoretical observations in oscillator networks, we hypothesize that human brains display a modular architecture for the explicit purpose of facilitating behavioral adaptability [13, 14]. Such a hypothesis is bolstered by evidence that neuronal cell distributions evolve differently in regions of the brain that code for simpler reflexive *versus* more complex adaptive functions [15]. The hypothesis also has specific implications for individual differences in cognitive ability across humans. Specifically, we expect that individuals that display greater modularity, or sparser connectivity, between neural units critical for task performance would also display more behavioral adaptability in the face of novel task demands [16, 17, 18] (Fig. 1b).

To test these hypotheses, we study a cohort of healthy adult human subjects who learn a new motor skill from visual cues over the course of 6 weeks (Fig. 1c). We acquire resting state fMRI data from each participant prior to task practice and model these data as whole-brain functional networks, where regions of the brain are represented as network nodes and statistical similarities, or synchronization, in regional activity are represented as network edges [19]. We extract the average activity in visual and motor regions that have previously been identified as key to evolving performance in this specific motor task [18], and quantify the functional integration between these two systems as the linear correlation between the two signals. We quantify motor skill learning as the reduction in the time required

to correctly execute a ten-element motor sequence, measured over the course of over 2000 trials per participant. We hypothesize that individuals who display a greater functional separation, or greater modularity, between motor and visual modules at rest are poised for enhanced adaptability, and therefore will learn faster over the 6 weeks of practice than individuals who display less functional separation between these modules. Further, we ask whether this baseline segregation between modules is a *trait* of an individual, consistently expressed over multiple scanning sessions, or a *state* of an individual, and therefore potentially vulnerable to external manipulation or internal self-regulation. The answers to these questions have direct implications for predicting and manipulating a human's ability to adapt its behavior — or learn — in the future.

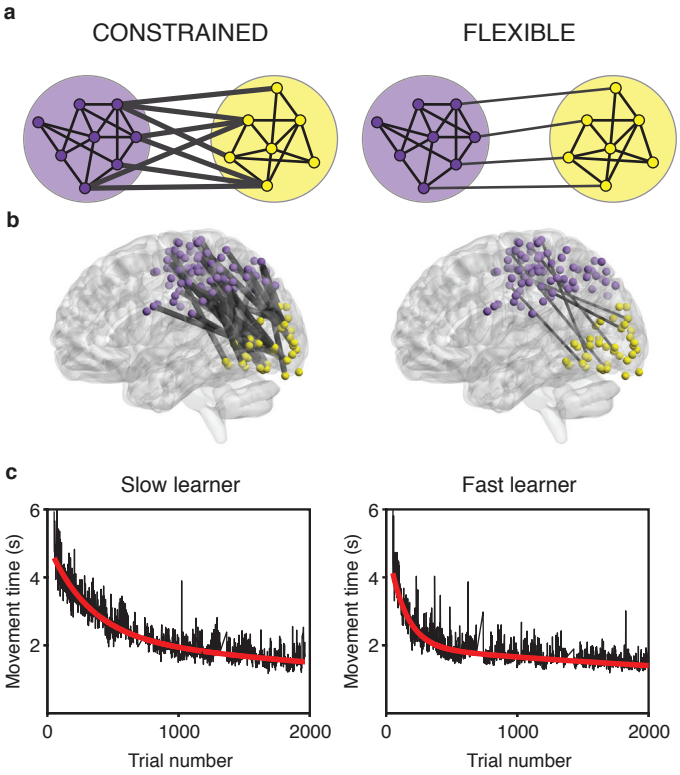


Figure 1: **Network dynamics constrain adaptive learning behavior.** *(a)* The degree of connectivity between two modules imposes constraints on the types of dynamics that are possible. Lower degrees of statistical dependence between the activity in two modules allow for greater flexibility in their dynamics. *(b)* Learning a new motor skill — a sequence of finger movements — induces a progressive change in the connectivity between visual and somato-motor cortices [18]. We hypothesize that individuals who display a greater functional separation, or greater modularity, between motor and visual modules at rest are poised for enhanced adaptability, and therefore will learn faster over the 6 weeks of practice than individuals who display less functional separation between these modules. *(c)* Time in seconds required to correctly perform each sequence of finger movements (here referred to as *movement time*) for two example human subjects over 6 weeks of training. We observe an exponential decay in the trial-by-trial movement times for all participants (black lines), indicating that learning is occurring. The exponential drop-off parameter of a two-term exponential fit (red line) quantifies how rapidly each participant learned. Left and right panels illustrate the fits for an example slow and fast learner, respectively.

# Results

## Behavioral markers of learning

Participants practiced a set of ten-element motor sequences in a discrete sequence-production (DSP) paradigm (Fig. S1). Training occurred over the course of 30 or more behavioral training sessions, spanning approximately 42 days (Fig. S2). The time required to correctly perform each sequence (movement time) decayed exponentially over time, and the rate of this decay displayed remarkable individual variability (Fig. 1c, S5). To quantify this feature of behavior, we defined the *learning rate* as the exponential drop-off parameter of the movement times, collated from home training sessions over the course of the entire experiment and averaged between two extensively practiced sequences (EXT sequences; see Methods) [18]. The learning rate – which quantifies how rapidly each participant converges to their own optimal performance – varied between $2.7 \times 10^{-3}$ and $8.0 \times 10^{-3}$ trial$^{-1}$ ($M = 5.2 \times 10^{-3}, SD = 1.6 \times 10^{-3}$ trial$^{-1}$). This indicates that the fastest learner converged to relatively steady performance approximately three times faster than the slowest learner (Fig. 1c).

## Sensorimotor initialization predicts future learning

Next, we asked whether a modular architecture during resting state - an important correlate of underlying structural connectivity [20, 21] and a marker of prior experience [22, 23, 24] – is predictive of behavioral adaptability. More specifically, we hypothesized that functional connections previously shown to change during the learning process [18] would, at baseline, explain individual variability in future learning rate.

To test this hypothesis, we measured spontaneous fluctuations in BOLD activity while participants underwent functional magnetic resonance imaging (fMRI), immediately prior to the initial task practice session. Our goal was to use these data to assess individual differences in the baseline strength of functional connections that displayed significant changes during task performance. We defined two modules and corresponding connections of interest (COI) based on task-based fMRI data from the same cohort. These two sets of regions, identified in prior work in a data-driven way [18], broadly corresponded to (i) early visual cortex (which has been referred to as the *visual module*; Fig. 2a) and (ii) primary and secondary somato-motor regions (*somato-motor module*; Fig. 2a). The two modules show significantly different time courses of blood oxygenation level-dependent (BOLD) activation during task practice, and become increasingly autonomous as a result of visuo-motor learning [18] (Table 1 shows region labels associated with the two modules). In order to verify whether these modules identified from task-based data were also effective modules at rest, we calculated the modularity quality of this partition during resting state (equation (2) in Methods). The value obtained for this partition was larger than the modularity calculated for all 10,000 partitions of equal size with randomly permuted regions ($P < 0.0001$), confirming that these sets of regions are also effective modules at rest.

We then asked whether gross interactions between these two modules at baseline were predictive of future learning rate. We extracted the average resting state time series across all regions from the visual module and across all regions from the motor module. We computed the Pearson correlation coefficient between these two time series, and

applied a Fisher $r$-to-$z$ transformation. We refer to this $z$-value as the *visual-motor connectivity*. We observed that individual differences in visual-motor connectivity in the resting state prior to any task practice predicted participant's future learning rate as estimated from the following 6 weeks of practice (Spearman's rank correlation: $\rho = -0.7158$, $P = 0.0008$; Fig. 2b). These results suggest that baseline visual-motor connectivity can be thought of as a sensorimotor initialization parameter that constrains adaptive learning behavior.

The relationship between resting visual-motor connectivity and future behavior was highly specific to learning rate, being unrelated to error rates, reaction time, or other parameters of the fitted movement time *versus* trials-practiced curve (Fig. S8). Moreover, the relationship remained significant even after regressing out the effect of initial performance (Spearman's rank correlation: $\rho = -0.7175$, $P = 0.0008$); after regressing out the effect of final performance (Spearman's rank correlation: $\rho = -0.5596$, $P = 0.0141$); or after regressing out the effects of both initial and final performances (Spearman's rank correlation: $\rho = -0.5632$, $P = 0.0135$). Therefore, baseline visual-motor connectivity is specifically related to the rate of decay of movement time (*learning rate*).

| **Visual module** | **Somato-motor module** |
|---|---|
| Left/Right intracalcarine cortex | Left/Right precentral gyrus |
| Left/Right cuneus cortex | Left/Right postcentral gyrus |
| Left/Right lingual gyrus | Left/Right superior parietal lobule |
| Left/Right supracalcarine cortex | Left/Right supramarginal gyrus, anterior |
| Left/Right occipital pole | Left/Right supplementary motor area |
| | Left parietal operculum cortex |
| | Right supramarginal gyrus, posterior |

Table 1: Brain areas in visual and somato-motor modules.

## Regional specificity of predictor

We then asked whether the predictive relationship between visual-motor connectivity and learning rate was regionally and behaviorally specific. Using a permutation procedure, we found that visual-motor connectivity was significantly more predictive of learning rate than connectivity between a randomized visual module and a randomized motor module ($P = 0.00006$; randomized modules are composed of random draws of brain regions — without replacement — of the same size as the real modules).

Having established that baseline functional connectivity between broadly defined visual and somato-motor areas predicts individual differences in future learning rate, we next explored which specific subregions — or functional connections — within visual and somato-motor areas might be most responsible for driving this effect. Using a surface-based parcellation in standard atlas space [25], we observed a general trend for negative correlations between visual-motor connectivity and learning rate, as evident from the predominantly blue color in Fig. 3a (Spearman's rank correlation between visual-motor connectivity and learning rate, using broad visual and somato-motor regions of interest from a surface-based parcellation, was: $\rho = -0.5596$, $P = 0.0141$). This indicates that the broader regions selected in surface space still retain the overall properties of the volumetric parcellation. To test whether some functional connections were significantly more correlated with learning rate than others, we used a bootstrap

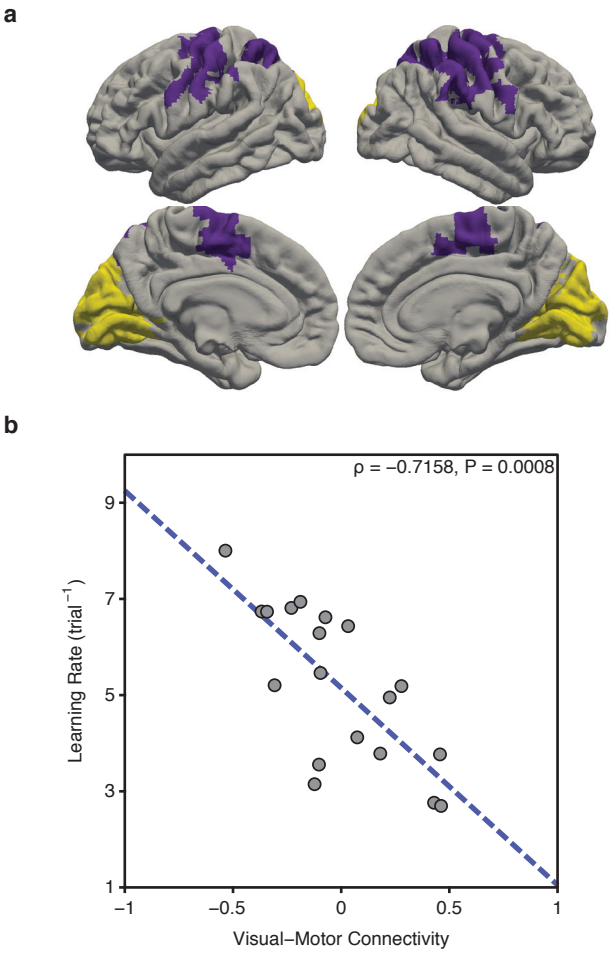


Figure 2: **Baseline Visual-Motor Connectivity Predicts Future Learning Rate.** *(a)* Visual module (yellow) and somato-motor module (purple), identified by time-resolved clustering methods applied to BOLD activity acquired during execution of motor sequences [18]. The modules were defined in a data-driven manner and correspond broadly but not exactly to putative visual and somato-motor modules. *(b)* Functional connectivity between visual and somato-motor modules, estimated at rest and prior to learning, reliably predicts individual differences in future learning rate. We define the learning rate as the exponential drop-off parameter of the participant's movement time as a function of trials practiced, and we define functional connectivity as the Fisher $r$-to-$z$ transformation of the Pearson correlation coefficient between regional average BOLD time series.

procedure with 10,000 subject samples with replacement to derive the sampling distribution of each correlation value in Fig. 3a. We observed that individual differences in future learning rate were most strongly predicted by functional connectivity between the premotor area adjacent to the right superior precentral sulcus and early-visual areas adjacent to the calcarine sulcus in both hemispheres (Left calcarine sulcus to right superior precentral sulcus: Spearman's $\rho = -0.8211$, bootstrap: $M = -0.7935$, 95% $CI = [-0.9365, -0.5434]$; Right calcarine sulcus to right superior precentral sulcus: Spearman's $\rho = -0.8228$, bootstrap: $M = -0.7904$, 95% $CI = [-0.9043, -0.6060]$; Fig. 3b,c). Across all bootstrap samples, these two values were larger than 98% of the others, demonstrating that these connections are robustly more correlated with learning rate than other visual-motor connections.

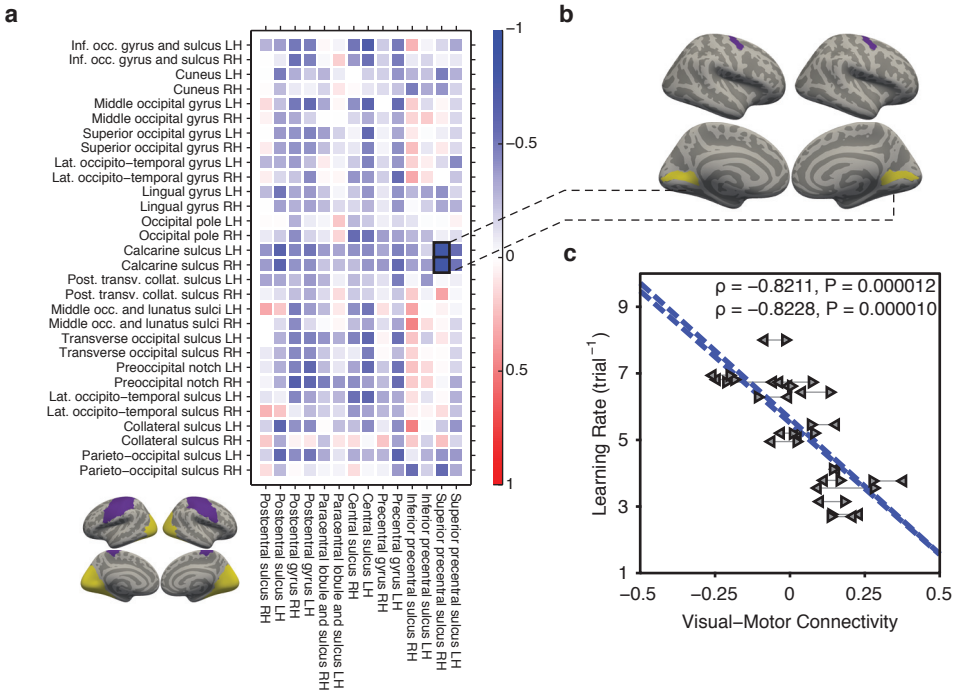


Figure 3: **Learning rate is best predicted by connectivity between early visual and dorsal premotor areas.** *(a)* Using a surface-based annotation encompassing broadly defined visual and somato-motor areas (inset in lower left), we calculated the correlation between learning rate and the functional connectivity between each pair of subregions (negative correlations are represented in blue; positive correlations are represented in red). Learning rate was best predicted by connectivity between early-visual areas adjacent to the calcarine sulcus in both hemispheres and the dorsal premotor area adjacent to the right superior precentral sulcus. *(b)* Regions whose connectivity were found to have highest correlation with learning rates. *Left*: Left calcarine sulcus (yellow) and right superior precentral sulcus (purple). *Right*: Right calcarine sulcus (yellow) and right superior precentral sulcus (purple). *(c)* Functional connectivity between left calcarine sulcus and right superior precentral sulcus significantly predicted individual differences in future learning rate ($\rho = -0.8211$, adjusted $P = 0.0051$; data points are indicated by left pointing triangles). Similarly, functional connectivity between right calcarine sulcus and right superior precentral sulcus significantly predicted learning rate ($\rho = -0.8228$, adjusted $P = 0.0042$; data points are indicated by right pointing triangles). P-values adjusted with Bonferroni correction at $\alpha = 0.05$.

## Sensorimotor initialization *versus* online control

The results described in the previous sections offer a parsimonious and simple explanation for individual differences in motor skill acquisition: namely that sensorimotor initialization constrains the flexible brain reconfiguration required for successful learning. Yet, such an explanation does not address the known role of higher-order cognitive processes

in sequence learning. Indeed, prior evidence suggests a critical role for online cognitive control – and its dynamic release [18] – during learning [26, 27] as well as adaptive behavior in general [28, 29]. Key control areas observed in motor skill learning include prefrontal cortex [26], anterior cingulate [18], and basal ganglia [30]. Are cognitive control processes only required *during* task performance, or can individual differences at baseline predict future learning?

To address this question, we focused on a circuit of interest identified in a data-driven manner from BOLD data collected as participants performed the task inside the scanner, composed of connections whose change in module allegiance throughout learning significantly correlates with individual differences in learning rate [18] (see Methods). This circuit is largely composed of connections between regions in the frontal cortex, anterior cingulate and basal ganglia including the nucleus accumbens and putamen (Fig. 4a). We observed that individual differences in the mean *baseline* strength of functional connections in the circuit of interest was not significantly correlated with future learning rate (Spearman's $\rho = -0.3965$, $P = 0.0939$, Fig. 4b). These results indicate that, while cognitive control is a critical driver of learning during task performance, baseline connectivity in this circuit of interest is statistically unrelated to future learning.

## Sensorimotor initialization: A state or a trait?

Given the predictive nature of baseline visual-motor connectivity, one might wish to know whether this baseline varies from day to day, thereby playing the role of an online initialization system, or whether it remains relatively stable over the course of the 6-week experiment. That is, are we measuring a network property related to learning that varies from session to session (over the course of hours to days) or is this a consistent relationship over the entire experiment, indicative of a trait effect? The answer to this question could offer much needed insight into the potential neurophysiological mechanisms underlying the observed relationship between baseline connectivity and learning: for example, from stable trait markers of structure [20, 21] or prior experience [22, 23, 24] to dynamic state markers of arousal [31].

To address this question, we measured spontaneous BOLD fluctuations in each of four resting state sessions conducted immediately prior to task execution and separated by 1.5–2 weeks over the 6 week training period. We calculated visual-motor connectivity and assessed the degree of inter-scan consistency using a random effects intraclass correlation coefficient, which we observed to be $ICC(C, 1) = 0.2395$ ($P = 0.0110$; Fig. 5a). These results indicate that approximately 24% of the observed variance in visual-motor connectivity was accounted for by differences between subjects (a *trait* marker), while 76% of the observed variance was accounted for by differences within subjects (which can include both measurement error and a potential *state* marker), varying from session to session. Importantly, there was no significant trend in the evolution of visual-motor connectivity across sessions (one-way analysis of variance, $F(3, 72) = 1.1624$, $P = 0.3301$).

How does the trait *versus* state nature of visual-motor connectivity impact prediction accuracy? We explicitly estimated the stable trait component by averaging an individual's visual-motor connectivity values over all four scanning sessions, and we observed that this trait component significantly predicts learning rate over the 6 weeks of

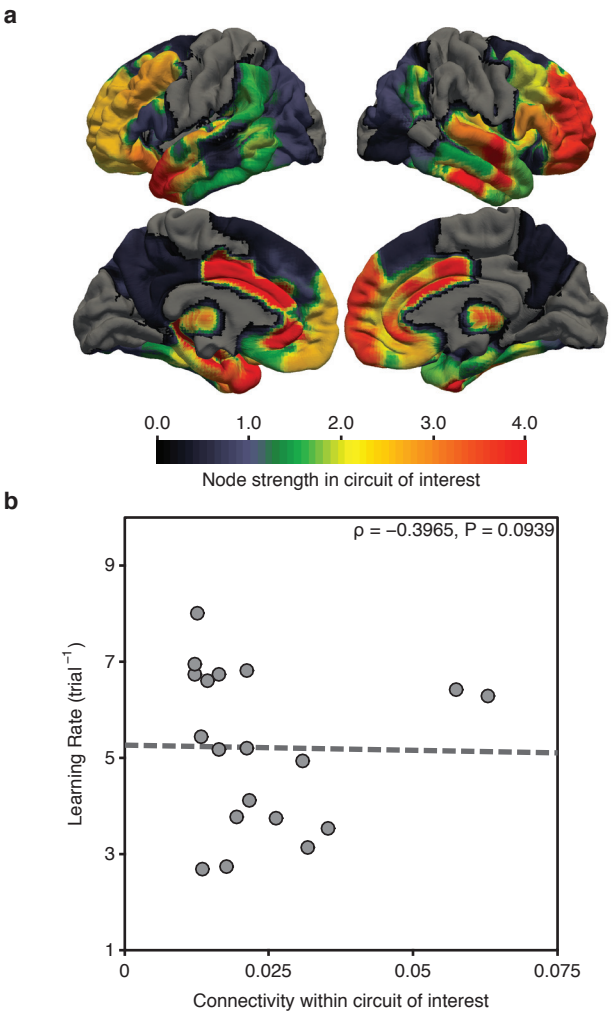


Figure 4: **Mean baseline connectivity within cognitive control areas does not correlate significantly with learning rate.** *(a)* Mean strength of areas from the circuit of interest, identified as the set of connections whose modulation over the course of the training period were significantly correlated ($p < 0.05$, uncorrected) with individual differences in learning rate [18]. This circuit largely corresponds to cognitive control areas, including regions in the frontal cortex, anterior cingulate and basal ganglia. *(b)* Mean baseline connectivity in connections from the circuit of interest prior to learning do not significantly correlate with individual differences in learning rate (Spearman's $\rho = -0.3965$, $P = 0.0939$; Pearson's $r = -0.0191$, $P = 0.9381$). A robust regression (using iteratively reweighted least squares with a bisquare weighting function) also indicated that the relationship was not significant ($P = 0.9484$), suggesting that the lack of correlation was not solely driven by outliers.

training (Spearman's $\rho = -0.5228$, $P = 0.0233$; Fig. 5b). Yet, there is clearly additional variance that is not explained by this trait component, as evidenced by session-to-session variability in visual-motor connectivity (Fig. 5a, S7).

To assess the potential predictive role of state dependent components of visual-motor connectivity, we asked whether visual-motor connectivity estimated from a single baseline scan predicts learning rate in a temporally adjacent training session more so than in temporally distant training sessions. Because of its exponentially decaying profile, learning rate is more robustly estimated early in training (see Fig. S9 for a demonstration). Therefore, we estimated a session-specific learning rate from movement times of minimally trained sequences. These trials were performed during scan sessions, in runs immediately following the resting state scans. While the individual correlations between session-specific learning rate and session-specific visual-motor connectivity were not statistically significant, their average ($\bar{\rho} = -0.29543$) was the largest of all possible pairings of resting state scans and task execution sessions (24 permutations, $P = 0.0400$). Importantly, the same result was obtained when the trait component was regressed out from the visual-motor connectivity at each session, indicating that the state component of visual-motor connectivity has a high temporal specificity. These results demonstrate that visual-motor connectivity contains both a trait and a state component, the former predicting a stable task aptitude and the latter predicting temporally-specific measures of learning.

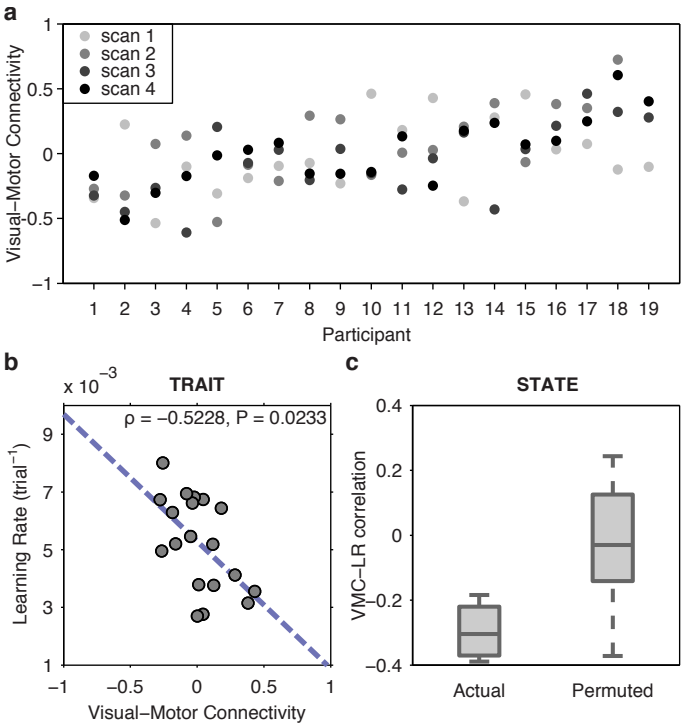


Figure 5: **Visual-motor connectivity as a trait and as a state.** *(a)* Between-session variability of visual-motor connectivity. For each participant, dots represent visual-motor connectivity measured at each of four resting state scans conducted immediately prior to task execution. Despite large variability between sessions, approximately 24% of the observed visual-motor connectivity variance was accounted for by a trait marker, representing between-subject variability. *(b)* By definition, the trait marker is the component of visual-motor connectivity that remains stable across time, with the variability from session to session here termed the *state* component. The average visual-motor connectivity across all four sessions, an estimator of the trait component of visual-motor connectivity, significantly predicted overall learning rate ($\rho = -0.5228, P = 0.02333$). *(c) Left:* Spearman's correlation coefficients between session-specific learning rate, estimated from trials performed inside the scanner immediately following resting state scans, and session-specific visual-motor connectivity. *Right*: Spearman's correlation coefficients for all 24 permutations of resting state scans to task sessions, between visual-motor connectivity and session-specific learning rates. The actual pairing of resting state scans to task sessions had the strongest average correlation from all possible pairings ($P = 0.0400$), indicating that the state component of visual-motor connectivity has a high temporal specificity.

# Discussion

While an understanding of many higher-level cognitive functions requires one to study the brain during effortful thought [32], some basic organizational principles and constraints can be observed while the brain idles at baseline. Consistent evidence from multiple imaging modalities and subject cohorts demonstrate that the brain's resting baseline is characterized by a modular [33, 14, 34], or near-decomposable nature [4], and that these modules are composed of brain regions that tend to perform similar cognitive functions [35, 36, 37, 38]. Yet, how this modular architecture supports the sequential and dynamic integration of the many high-level cognitive functions required during motor skill learning remains far from understood [39]. Here we observe that individuals who display lower values of correlation between their resting baseline activity in motor and visual regions learn faster in the following 6 weeks of task practice. That is: more modular architecture at rest is benefitial for learning in the future. This result complements both empirical and theoretical lines of inquiry recently demonstrating that modular architecture confers robustness as well as evolvability simultaneously [40], helps organisms evolve new skills without forgetting old skills [41], and – in the motor-visual systems – increases as learning occurs [18].

**The Benefits of Independence.** While the baseline separation between entire motor and visual modules was predictive of individual differences in future learning behavior over 6 weeks of task practice, we also observed that the regional associations that drove this prediction most were the functional connections between the contralateral superior precentral sulcus and the bilateral calcarine sulcus. In classical models of motor processing and control, the superior precentral sulcus is thought of as the dorsal premotor area [42], and activation in this area is related to the performance of visuomotor hand/arm conditional responses [43]. It is well know that this region plays a central role in mapping visual cues to spatial motor responses in both human and non-human primates [44, 45, 46, 47, 48]. Given this specific role in motor-visual integration, it is interesting that individuals with the weakest baseline connections between this area and early visual cortices learn the fastest. One simple interpretation of these findings builds on the notion that the learning process is one in which the task of the brain is to develop direct motor-motor associations [49, 50]: each finger movement directly triggers the next, without the need for visual cues. Individuals with low connectivity between dorsal premotor and visual areas – and therefore more independence or autonomy of visual and motor processes [18] – are able to develop motor-motor associations faster.

Such an explanation suggests the presence of a broader competitive process that may play a role in other cognitive tasks: individuals that display greater integration between cognitive processes at rest may be less able to disengage such processes from one another during task execution. This hypothesis is indeed supported by preliminary evidence in both healthy and clinical cohorts. For example, in healthy adult subjects, increased modularity (decreased integration) of resting state functional connectivity networks has been shown to be positively correlated with improvement in attention and executive function after cognitive training [51]. Similarly, individuals with greater negative correlation between default mode and working memory networks exhibited better behavioural performance on a working memory task [52]. Conversely, in subcortical vascular mild cognitive impairment, increased integration between modules in the

inferior and superior parietal gyrus at rest has been shown to be associated with impaired cognitive performance [53]. Finally, such a broad competitive process is supported by recent work in normative neurodevelopment showing that individuals with weaker sensorimotor integration at rest tended to display better cognitive performance ($N = 780$ in the Philadelphia Neurodevelopmental Cohort) [54].

**Drivers of Baseline Architecture.** A growing literature demonstrates the absolutely fundamental role of baseline network architecture in explaining individual differences in cognition and behavior. The strength of individual functional connections, or larger sets of connections, have been observed to correlate with individual differences in IQ [55], visual orientation discrimination [56], working memory [52, 57], color knowledge [58], auditory stimulus detection [59], pursuit rotor performance [60], and the ability to learn foreign sounds [61] and probabilistic regularities [62]. Yet, it is unclear what neurophysiological or develpmental factors drive these individual differences at baseline.

Current theories of resting state drivers can be summarized along two key dimensions: genetically-encoded structure, and prior or current experience. First, resting state functional connectivity is related to some degree to underlying large-scale structural connectivity as estimated by white matter tractography [20, 63, 64, 21, 65]: two brain areas that are connected by a large number of white matter streamlines also tend to display strong correlations in their resting BOLD activity. These structural patterns may form a constraint on resting state dynamics, at least partially driven by the genetic codes underlying module formation [66]. Yet, structural connectivity can only be a partial explanation, as resting state functional connectivity varies appreciably over time scales in which structure remains constant [67, 68, 69, 70]. It will be interesting in future to determine whether structural differences among individuals might explain some of the predictive relationship between resting state functional connectivity and future learning behavior.

The second key driver of resting state functional connectivity is experience. Over short time scales, resting state patterns are altered for up to 20 minutes following task performance [71], being modulated by cognitive processes as diverse as short term memory [72] and visuomotor learning [73]. Moreover, resting state connectivity can be altered over longer time scales with cognitive training [51], mindfulness training [22, 74], progressive neurological disorders [75], and aging [76]. While recent and more distant experience can play a role, perhaps the more tantalizing observation is that a person's arousal state is also directly linked to their resting state functional connectivity [77]. This finding is particularly interesting in light of our results from the state-trait analysis, which indicate that visuomotor connectivity is more correlated with learning occurring in the immediately following trials than with trials performed in a different session. These state-dependent predictors of future learning are consistent with recent work demonstrating that arousal systems may directly regulate learning by coordinating activity in the locus coeruleus and anterior cingulate cortex [31]. Future work is necessary to determine the degree to which arousal state – as opposed to prior training – might manipulate the pattern of resting state connectivity, priming the system to optimally learn in the immediate future.

**Baseline Initializations vs. Transient, Online Control.** While cognitive control is a critical driver of learning during task performance [78, 26, 79, 18], we observe that baseline functional connections within this circuit do not significantly correlate with individual differences in future learning. This finding nuances our understanding of the relative importance of (i) baseline architecture, which represents the initialization of the brain, and (ii) task-elicited dynamics, which represents transient, online control. In combination with prior literature, our results suggest that the relative autonomy of sensorimotor systems at rest is followed by flexible alterations in the functional circuitry of cognitive control regions as the task is executed [18], strengthening the motor-motor associations that enable automatic performance [49, 50].

**Methodological Considerations.** There are several important methodological and conceptual considerations relevant to this work. First, while we use the term *modularity*, we do not mean the tradition notion of pure encapsulation of function as propounded by Fodor in his historic contribution to the field: "Modularity of Mind" [80]. Instead, we use the term as mathematically defined in [81] to mean separation or segregation without requiring complete independence. Second, it is important to determine the specificity of the findings. We note that the degree of connectivity between visual and somato-motor areas predict learning rate but not other metrics of task performance, and that this effect does not generalize to a cognitive control circuit defined *a priori* from task-based fMRI data collected while the same participants performed the DSP paradigm. Third, it is important to be clear about what the estimate of learning rate used here measures and what it does not measure. Critically, the learning rate is independent of initial performance, a measurement of experience on similar tasks, and is independent of final performance, a measurement of finger mechanics. Finally, in this work, we utilize large-scale non-invasive human recording of BOLD signals across cortical, subcortical, and cerebellar areas. It would be interesting in future to determine whether the sensorimotor autonomy that we describe here is related to competitive sensorimotor interactions reported at the neuronal level [82].

**Implications for Educational and Clinical Neuroscience.** We have shown that baseline visuo-motor connectivity is a strong predictor of learning rate specifically in a DSP paradigm, but it is possible that these results would generalize to other motor skills, or that baseline separation between relevant cognitive systems is, in general, beneficial for other classes of learning in perceptual, cognitive or semantic domains. Predicting individual differences in future learning has massive implications for neurorehabilitation (in those who are aging, injured or diseased) and neuroeducation (in children or older trainees). Predictors drawn from behavioral performance or from brain images acquired during behavioral performance necessarily have limited applicability in rehabilitation and education domains where subjects may be unable to perform the task, or be unable to lie still in a scanner during task performance. Predictors drawn from resting state scans offer the possibility for direct translation to the clinic and classroom. Moreover, our delineation of state and trait components of sensorimotor initialization predictors suggests the possibility of directly manipulating subject state, for example with non-invasive stimulation [26, 83], neurofeedback, or task priming [84] to enhance future performance, thereby optimizing rehabilitation or training.

# Methods

## Participants

Twenty-two right-handed participants (13 females and 9 males; mean age of 24 years) volunteered to participate in this study. All volunteers gave informed consent in writing, according to the guidelines of the Institutional Review Board of the University of California, Santa Barbara. Three participants were excluded: one failed to complete the experiment, one had excessive head motion, and one had a functional connectivity profile whose dissimilarity to those obtained from other participants was more than three standard deviations away from the mean, potentially due to sleep (Fig. S4). Therefore, the final cohort included 19 participants who all had normal or corrected vision and no history of neurological disease or psychiatric disorders.

## Experimental setup and procedure

In a discrete sequence-production (DSP) task, participants practiced a set of ten-element motor sequences either on a laptop keyboard, responding to sequential visual stimuli using their right hand (Fig. S1). The visual display contained a horizontal array of five square stimuli, each corresponding to one finger. Mapped from left to right, the thumb corresponded to the leftmost stimulus and the smallest finger corresponded to the rightmost stimulus. The square corresponding to the current button press was highlighted in red, changing to the next square immediately following a correct button press. Only correct button presses advanced the sequence, and the time for completion was not limited. Participants were instructed to respond quickly and to maintain accuracy.

Six different ten-element sequences were used in the training protocol, with three possible levels of exposure: two sequences were extensively trained (EXT; 64 trials per session); two sequences were moderately trained (MOD; 10 trials per session); and two sequences were minimally trained (MIN; 1 trial per session). The same sequences were practiced by all participants. In each sequence, each of the five possible stimulus location was presented twice and included neither immediate repetitions (e.g. "1-1") nor regularities such as trills (e.g., "1-2-1") or runs (e.g., "1-2-3"). A sequence-identity cue indicated, on each trial, what sequence the participant was meant to produce: EXT sequences were preceded by either a cyan (EXT-1) or a magenta (EXT-2) circle, MOD sequences were preceded by either a red (MOD-1) or a green (MOD-2) triangle, and MIN sequences were preceded by either an orange (MIN-1) or a white (MIN-2) star. No participant reported any difficulty viewing the identity cues. The number of error-free sequences produced and the mean time required to complete an error-free sequence was presented after every block of ten trials. See Fig. S3 for the number of trials performed for each sequence type.

Participants were scanned on the first day of the experiment (scan 1) and on three other occasions (scans 2–4) spaced approximately 1.5–2 weeks from one another. The entire experiment spanned approximately a 42-day period (Fig. S2). A minimum of ten home training sessions was completed in between any two successive scanning sessions, for a total of at least 30 home sessions. Home training sessions were performed on personal laptop computers using a training module installed by the experimenter.

Before the first scanning session, the experimenter provided a brief introduction to participants in which he explained the mapping between the fingers and the DSP stimuli, as well as the significance of the identity cues. Next, fMRI data was acquired as Subjects rested quietly in the scanner prior to any task performance. Finally, fMRI data was acquired as subjects performed a series of trials on the DSP task spread over five scan runs, using a 5-button button box with distances between keys similar to placement on a standard 15in laptop. Each scan run acquired during task performance contained 60 trials grouped in blocks of ten, and similarly to home training sessions, performance feedback was given at the end of every block. Each block contained trials belonging to a single exposure type (EXT, MOD or MIN), and included five trials for each of the two sequences. Therefore, an equal number of trials from each sequence was performed during scan sessions (50 trials per sequence, for a total of 300 trials per scan session; Fig. S3). Trial completion was indicated by a fixation cross, which remained on the screen until the onset of the next sequence identity cue (the intertrial interval varied between 0 and 6s).

Two sessions were abbreviated due to technical challenges. In each case when a scan was cut short, participants completed four out of the five scan runs for a given session. We included behavioral data from these abbreviated sessions in this study.

## Behavioral apparatus

In home train sessions, stimuli were presented with Octave 3.2.4 and Psychtoolbox 3 [85] on each participants' laptop computer. During scanning sessions, stimuli were presented with MATLAB version 7.1 (Mathworks, Natick, MA) and Psychtoolbox 3 [85], backprojected onto a screen and viewed through a mirror. Key-presses and response times were collected using a custom fiber optic button box and transducer connected via a serial port (button box, HHSC-1 $\times$ 4-l; transducer, fORP932; Current Designs, Philadelphia, PA), with design similar to those found on typical laptops. For instance, the center-to-center spacing between the buttons on the top row was 20 mm (compared to 20 mm from "G" to "H" on a recent version of the MacBook Pro), and the spacing between the top row and lower left "thumb" button was 32 mm (compared to 37 mm from "G" to the spacebar on a MacBook Pro).

## Behavioral estimates of learning

Consistent with convention, we defined the movement time ($MT$) as the difference between the time of the first button press and the time of the last button press in a single sequence. We calculated $MT$ for every sequence performed in home training sessions over the course of the 6 weeks of practice. Across all trials in home training sessions, the median movement time was, on average, 1.70 s (average minimum 1.03 s and average maximum 7.12 s), with an average standard deviation of 0.79 s. For each participant and each sequence, the movement times were fit with a two-term exponential model [86, 87] using robust outlier correction (using MATLAB's function "fit.m" in the Curve Fitting Toolbox with option "Robust" and type "LAR"), according to the equation (1).

$$MT = D_1 e^{t\kappa} + D_2 e^{t\lambda}, \tag{1}$$

where $t$ is time, $\kappa$ is the exponential drop-off parameter (which we refer to as the *learning rate*) used to describe the fast rate of improvement, $\lambda$ is the exponential drop-off parameter used to describe the slow, sustained rate of improvement, and $D_1$ and $D_2$ are real and positive constants. The magnitude of $\kappa$ indicates the steepness of the learning curve: curves with larger $\kappa$ values decay more quickly than curves with smaller $\kappa$ values. Therefore, $\kappa$ indicates the speed of learning independently of initial performance or performance ceiling. The decrease in movement times has been used to quantify learning for several decades [88, 89]. Several functional forms have been suggested for the fit of movement times [90, 91], and variants of an exponential are viewed as the most statistically robust choices [91]. Given the vastly superior number of practiced trials in EXT sequences (Fig. S3), we estimate the *learning rate* for each participant as the average $\kappa$ between both EXT sequences, consistent with previous work [18].

In addition to movement time, we defined *error rate* as the number of incorrect button presses during the full execution of each sequence, and *reaction time* as the time between the onset of a trial and the first button press. We performed a linear fit on both of these additional measures and repeated our main analysis with both their intercept and slope terms (Fig. S8).

## MRI Data collection

Magnetic resonance images were obtained at $3.0T$ on a Siemens Trio using a 12-channel phased-array head coil. T1-weighted structural images of the whole brain were collected from each subject (repetition time $[TR] = 15.0ms$; time echo $[TE] = 4.2ms$; flip angle: 90°; 3D acquisition; field of view: $256mm$, slice thickness: $0.89mm$; $256 \times 256$ acquisition matrix). Data from one resting state run (146 TRs), five experimental runs (variable number of TRs depending on how quickly the task was performed [18]), and a second resting state run (146 TRs) were acquired with a single-shot echo planar imaging sequence that was sensitive to BOLD contrast ($[TR] = 2,000ms$; time echo $[TE] = 30ms$; flip angle: 90°; field of view: $192mm$, slice thickness: $3mm$ with $0.5mm$ gap; $64 \times 64$ acquisition matrix across 37 axial slices per TR).

## MRI Data preprocessing

Cortical reconstruction and volumetric segmentation of the structural data was performed with the Freesurfer image analysis suite [92]. Preprocessing of the resting state fMRI data involved multiple steps: the first four volumes in each run were discarded to allow stabilization of longitudinal magnetization; sinc-interpolation in time was performed with AFNI's [93] 3dTshift to correct for the slice acquisition order; orientation of all images was changed to Right-Posterior-Inferior using AFNI's 3dresample; images were rigid-body motion corrected with AFNI's 3dvolreg by aligning all volumes with the mean volume (estimated with AFNI's 3dTstat) in each run; coregistration between structural and mean functional image was performed with Freesurfer's bbregister [94]; brain-extracted functional images were obtained by applying Freesurfer's brain mask on to images from each functional run using AFNI's 3dcalc; global intensity normalization was performed across all functional volumes using FSL's fslmaths [95] to ensure that all time series were in the same units; functional data was smoothed in surface space with an isotropic Gaussian kernel of

5-mm full width at half-maximum and in the volumetric space with an isotropic Gaussian kernel of 5-mm full width at half-maximum and, using Freesurfer's `mris_volsmooth`; intensity and motion outliers were detected using Artifact Detection Tools (ART) [96] and removed from time-series using a regression approach; the six motion parameters (three for translation and three for rotation) estimated with ART, as well as the temporal derivatives, quadratic terms, and temporal derivatives of the quadratic terms had also their contribution removed from the BOLD signal; non-neuronal sources of noise (white-matter and CSF signals) were estimated by averaging signals within masks obtained with Freesurfer segmentation tools and by identifying voxel time series with high temporal standard deviations, and removed using the anatomical (aCompCor) and temporal CompCor (tCompCor) methods [97]; finally, a temporal band-pass filter of 0.01 Hz to 0.1 Hz was applied using AFNI's 3dFourier. Global signal was not regressed out of voxel time series due to its controversial application to resting state fMRI data [98, 99, 100].

Using the above processing pipeline, we expect to have been able to correct for motion effects due to volume-to-volume fluctuations relative to the first volume in a scan run. After this motion-correction procedure, we observed no correlation between any of the six motion parameters (x-translation, y-translation, z-translation, roll, pitch and yaw, calculated for each run and training session) and visual-motor connectivity ($P > 0.05$) across all scanning sessions. These results indicated that individual differences in motion were unlikely to drive the effects reported here.

## Parcellation scheme

We used a volumetric-based parcellation scheme composed of 626 regions of interest (ROIs) that was formed by the combination of two separate atlases: (i) an AAL-derived 600-region atlas [63, 64], which subdivides the 90 AAL anatomical regions into regions of roughly similar size via a spatial bisection method, and (ii) a high-resolution probabilistic 26-region atlas of the cerebellum in the anatomical space defined by the MNI152 template, obtained from T1-weighted MRI scans (1-mm isotropic resolution) of 20 healthy young participants [95, 103] (note that this latter atlas is provided by SPM8). The combination of these two atlases provided a high-resolution, 626-region atlas of cortical, subcortical, and cerebellar regions. This volumetric atlas, which we call AAL-626 atlas, have been used previously [18]. The surface-based analyses used an automatic parcellation of human cortical gyri and sulci (Freesurfer's aparc.a2009) [25].

## Functional Connectivity estimation

In previous work, analyses of the task data from the same experiment yielded two sets of ROIs from the AAL-626 atlas based on the high probability that its regions were assigned to the same functional community by time-resolved clustering methods [18]. These two sets of regions broadly corresponded to (i) early visual cortex (which has been referred to as the *visual module*; Fig. 2a) and (ii) primary and secondary somato-motor regions (*somato-motor module*; Fig. 2a). A list of region labels associated with the two modules is displayed in Table 1. We extracted the average resting state time series across regions from each of the functional modules, calculated their Spearman's rank correlation coefficient (a nonparametric measure of statistical dependence between two variables), and applied a

Fisher $r$-to-$z$ transformation. We refer to this $z$-value as the *visual-motor connectivity*.

Importantly, the removal of various signal components present throughout most of the brain (in particular by the tCompCor method) leads to a shift on the distribution of functional connectivity values, giving rise to negative correlations. We note that, while these approaches substantially improve the robutsness of our results by eliminating physiological noise from the data [104], our results remain significant with a less stringent noise removal pipeline that does not shift the range correlation values (Fig. S6).

We confirmed that the modules identified from the task data were also modules at baseline by comparing the modularity quality [105] of the actual partition with the modularity quality of $10,000$ permuted partitions. The modularity quality is given by equation (2):

$$Q = \frac{1}{4m} \sum_{ij} \left( A_{ij} - \frac{k_i k_j}{2m} \right) \delta(g_i, g_j), \tag{2}$$

where $A_{ij}$ is the functional connectivity matrix including all visual and motor regions, $k_i$ and $k_j$ are the strength of nodes $i$ and $j$, $m = \frac{1}{2}\sum_i k_i$ is the total strength in the network, and $\delta(g_i, g_j) = 1$ if nodes $i$ and $j$ belong to the same module or $\delta(g_i, g_j) = 0$ otherwise. We observed that the modularity quality of the actual partition into visual and motor modules was higher than the modularity quality of all $10,000$ permuted partitions ($p = 0.0001$), demonstrating that the separation of brain regions into motor and visual modules is an accurate representation of the network organization.

A similar approach was performed for the surface-based analysis, which aimed to identify which specific functional connections within visual and somato-motor areas were most correlated with learning rate. We used broadly defined visual and somato-motor regions of interest (ROIs) and examined the correlations between each visual-to-motor connection and learning rate. The visual ROI was defined as composed of the entire occipital lobe, parieto-occipital, and occipito-temporal areas (Fig. 3a), and the somato-motor ROI was defined as composed of precentral, paracentral and postcentral sulci and gyri, and central sulcus (Fig. 3a). After projecting the BOLD time-series from each voxel into surface vertices in subject native space, we extracted the average activity within each of the surface-based parcels and calculated the Fisher $r$-to-$z$ transformation of the Spearman's rank correlation coefficient between the activity in each region of the visual ROI and each region of the somato-motor ROI.

The fronto-cingulate cognitive control circuit of interest from Fig. 4a was defined from prior work [18], comprising data collected as participants performed the task inside the scanner and parcellated into 112 cortical and subcortical regions using the Harvard-Oxford (HO) atlas of the FMRIB (Oxford Centre for Functional Magnetic Resonance Imaging of the Brain) Software Library [95, 103] (FSL; Version 4.1.1). The circuit was defined as the set of edges connecting non-visual and non-motor areas whose modulation in module allegiance over the 6-week period was significantly correlated with learning rate. It was composed of 180 functional connections distributed asymmetrically throughout the network, with few brain areas having most of the connections and most areas having only a few. We converted each connection of the circuit of interest from the HO atlas to the AAL-626 atlas by identifying the region

in AAL-626 with the largest volumetric overlap with each region of HO and connecting corresponding pairs of regions with the appropriate edge strength. A visualization of the sum of the weights of the edges emanating from each area in AAL-626 is illustrated in Fig. 4a.

## Measure of statistical relationship

Spearman's rank correlation was chosen as a measure of statistical relationship between any two variables with different units. This nonparametric statistic measures the extent to which two variables are monotonically related without a requirement for linearity. To assess the relationship between two variables with the same units, Pearson product-moment correlation was used.

# References

[1] Kirschner M, Gerhart J (1998) Evolvability. *Proc Natl Acad Sci USA* 95(15):8420–8427.

[2] Kashtan N, Alon U (2005) Spontaneous evolution of modularity and network motifs. *Proceedings of the National Academy of Sciences of the United States of America* 102(39):13773–13778.

[3] Félix MA, Wagner A (2008) Robustness and evolution: concepts, insights and challenges from a developmental model system. *Heredity* 100(2):132–140.

[4] Simon HA (1962) The architecture of complexity', reprinted in simon (1969). *Simon84The Architecture of Complexity1962* pp. 84–118.

[5] Wagner GP, Altenberg L (1996) Complex adaptations and the evolution of evolvability. *Evolution* 50:967–976.

[6] Schlosser G, Wagner GP (2004) *Modularity in development and evolution.* (University of Chicago Press).

[7] Mallarino R et al. (2011) Two developmental modules establish 3D beak-shape variation in Darwin's finches. *Proc Natl Acad Sci U S A* 108(10):4057–4062.

[8] Koyabu D et al. (2014) Mammalian skull heterochrony reveals modular evolution and a link between cranial development and brain size. *Nature communications* 5.

[9] Fries P (2005) A mechanism for cognitive dynamics: neuronal communication through neuronal coherence. *Trends in cognitive sciences* 9(10):474–480.

[10] Voytek B et al. (2015) Oscillatory dynamics coordinating human frontal networks in support of goal maintenance. *Nat Neurosci* 18(9):1318–1324.

[11] Gomez-Gardenes J, Moreno Y, Arenas A (2007) Paths to synchronization on complex networks. *Phys Rev Lett* 98(3):034101.

[12] Arenas A, Díaz-Guilera A, Pérez-Vicente CJ (2006) Synchronization reveals topological scales in complex networks. *Physical review letters* 96(11):114102.

[13] Meunier D, Lambiotte R, Bullmore ET (2010) Modular and hierarchically modular organization of brain networks. *Front Neurosci* 4:200.

[14] Bullmore E et al. (2009) Generic aspects of complexity in brain imaging data and other biological systems. *Neuroimage* 47(3):1125–1134.

[15] Lewitus E, Hof PR, Sherwood CC (2012) Phylogenetic comparison of neuron and glia densities in the primary visual cortex and hippocampus of carnivores and primates. *Evolution* 66(8):2551–2563.

[16] Bassett DS et al. (2011) Dynamic reconfiguration of human brain networks during learning. *Proceedings of the National Academy of Sciences* 108(18):7641–7646.

[17] Bassett DS et al. (2013) Task-based core-periphery organization of human brain dynamics. *PLoS Comput Biol* 9(9):e1003171.

[18] Bassett DS, Yang M, Wymbs NF, Grafton ST (2015) Learning-induced autonomy of sensorimotor systems. *Nature neuroscience* 18(5):744–751.

[19] Bullmore ET, Bassett DS (2011) Brain graphs: graphical models of the human brain connectome. *Annu Rev Clin Psychol* 7:113–140.

[20] Honey CJ et al. (2009) Predicting human resting-state functional connectivity from structural connectivity. *Proc Natl Acad Sci U S A* 106(6):2035–2040.

[21] Goñi J et al. (2014) Resting-brain functional connectivity predicted by analytic measures of network communication. *Proc Natl Acad Sci U S A* 111(2):833–838.

[22] Taylor VA et al. (2012) Impact of meditation training on the default mode network during a restful state. *Social cognitive and affective neuroscience* p. nsr087.

[23] Duan X et al. (2012) Reduced caudate volume and enhanced striatal-dmn integration in chess experts. *Neuroimage* 60(2):1280–1286.

[24] Burton H, Snyder AZ, Raichle ME (2014) Resting state functional connectivity in early blind humans. *Front Syst Neurosci* 8:51.

[25] Destrieux C, Fischl B, Dale A, Halgren E (2010) Automatic parcellation of human cortical gyri and sulci using standard anatomical nomenclature. *Neuroimage* 53(1):1–15.

[26] Galea JM, Albert NB, Ditye T, Miall RC (2010) Disruption of the dorsolateral prefrontal cortex facilitates the consolidation of procedural skills. *Journal of cognitive neuroscience* 22(6):1158–1164.

[27] Chrysikou EG, Weber MJ, Thompson-Schill SL (2014) A matched filter hypothesis for cognitive control. *Neuropsychologia* 62:341–355.

[28] Chrysikou EG, Novick JM, Trueswell JC, Thompson-Schill SL (2011) The other side of cognitive control: can a lack of cognitive control benefit language and cognition? *Top Cogn Sci* 3(2):253–256.

[29] Thompson-Schill SL, Ramscar M, Chrysikou EG (2009) Cognition without control: When a little frontal lobe goes a long way. *Curr Dir Psychol Sci* 18(5):259–263.

[30] Orban P et al. (2010) The multifaceted nature of the relationship between performance and brain activity in motor sequence learning. *Neuroimage* 49(1):694–702.

[31] Nassar MR et al. (2012) Rational regulation of learning dynamics by pupil-linked arousal systems. *Nature neuroscience* 15(7):1040–1046.

[32] Gazzaniga MS, Mangun GR, eds. (2014) *The Cognitive Neurosciences*. (MIT Press).

[33] Meunier D, Achard S, Morcom A, Bullmore E (2009) Age-related changes in modular organization of human brain functional networks. *Neuroimage* 44(3):715–723.

[34] Sporns O, Betzel RF (2015) Modular brain networks. *Annu Rev Psychol* Sep 21.

[35] Salvador R, Suckling J, Schwarzbauer C, Bullmore E (2005) Undirected graphs of frequency-dependent functional connectivity in whole brain networks. *Philos Trans R Soc Lond B Biol Sci* 360(1457):937–946.

[36] Power JD et al. (2011) Functional network organization of the human brain. *Neuron* 72(4):665–678.

[37] Yeo BT et al. (2011) The organization of the human cerebral cortex estimated by intrinsic functional connectivity. *J Neurophysiol* 106(3):1125–1165.

[38] Cole MW, Bassett DS, Power JD, Braver TS, Petersen SE (2014) Intrinsic and task-evoked network architectures of the human brain. *Neuron* 83(1):238–251.

[39] Medaglia JD, Lynall ME, Bassett DS (2015) Cognitive network neuroscience. *J Cogn Neurosci* 27(8):1471–1491.

[40] Anderson ML, Finlay BL (2014) Allocating structure to function: the strong links between neuroplasticity and natural selection. *Front Hum Neurosci* 7:918.

[41] Ellefsen KO, Mouret JB, Clune J (2015) Neural modularity helps organisms evolve to learn new skills without forgetting old skills. *PLoS Comput Biol* 11(4):e1004128.

[42] Hardwick RM, Rottschy C, Miall RC, Eickhoff SB (2013) A quantitative meta-analysis and review of motor learning in the human brain. *Neuroimage* 67:283–297.

[43] Amiez C, Kostopoulos P, Champod AS, Petrides M (2006) Local morphology predicts functional organization of the dorsal premotor region in the human brain. *The Journal of neuroscience* 26(10):2724–2731.

[44] Astafiev SV et al. (2003) Functional organization of human intraparietal and frontal cortex for attending, looking, and pointing. *J Neurosci* 23(11):4689–4699.

[45] Rushworth MF, Johansen-Berg H, Gobel SM, Devlin JT (2003) The left parietal and premotor cortices: motor attention and selection. *Neuroimage* 20(Suppl 1):S89–100.

[46] Grefkes C, Fink GR (2005) The functional organization of the intraparietal sulcus in humans and monkeys. *J Anat* 207(1):3–17.

[47] Halsband U, Lange RK (2006) Motor learning in man: a review of functional and clinical studies. *Journal of Physiology-Paris* 99(4):414–424.

[48] Kravitz DJ, Saleem KS, Baker CI, Mishkin M (2011) A new neural framework for visuospatial processing. *Nat Rev Neurosci* 12(4):217–230.

[49] Verwey WB (2001) Concatenating familiar movement sequences: the versatile cognitive processor. *Acta Psychol (Amst)* 106(1–2):69–95.

[50] Wymbs NF, Bassett DS, Mucha PJ, Porter MA, Grafton ST (2012) Differential recruitment of the sensorimotor putamen and frontoparietal cortex during motor chunking in humans. *Neuron* 74(5):936–946.

[51] Arnemann KL et al. (2015) Functional brain network modularity predicts response to cognitive training after brain injury. *Neurology* 84(15):1568–1574.

[52] Sala-Llonch R et al. (2012) Brain connectivity during resting state and subsequent working memory task predicts behavioural performance. *Cortex* 48(9):1187–1196.

[53] Yi LY et al. (2015) Disrupted topological organization of resting-state functional brain network in subcortical vascular mild cognitive impairment. *CNS Neurosci Ther* 21(10):846–854.

[54] Gu S et al. (2015) Emergence of system roles in normative neurodevelopment. *Proc Natl Acad Sci U S A* Epub ahead of print.

[55] Santarnecchi E, Tatti E, Rossi S, Serino V, Rossi A (2015) Intelligence-related differences in the asymmetry of spontaneous cerebral activity. *Human brain mapping* 36(9):3586–3602.

[56] Baldassarre A et al. (2012) Individual variability in functional connectivity predicts performance of a perceptual task. *Proceedings of the National Academy of Sciences* 109(9):3516–3521.

[57] Zou Q et al. (2013) Intrinsic resting-state activity predicts working memory brain activation and behavioral performance. *Hum Brain Mapp* 34(12):3204–3215.

[58] Wang X et al. (2013) Where color rests: spontaneous brain activity of bilateral fusiform and lingual regions predicts object color knowledge performance. *NeuroImage* 76:252–263.

[59] Sadaghiani S, Poline JB, Kleinschmidt A, DEsposito M (2015) Ongoing dynamics in large-scale functional connectivity predict perception. *Proceedings of the National Academy of Sciences* 112(27):8463–8468.

[60] Wu J, Srinivasan R, Kaur A, Cramer SC (2014) Resting-state cortical connectivity predicts motor skill acquisition. *NeuroImage* 91:84–90.

[61] Ventura-Campos N et al. (2013) Spontaneous brain activity predicts learning ability of foreign sounds. *The Journal of Neuroscience* 33(22):9295–9305.

574 [62] Stillman CM et al. (2013) Caudate resting connectivity predicts implicit probabilistic sequence learning. *Brain*
575 *connectivity* 3(6):601–610.

576 [63] Hermundstad AM et al. (2013) Structural foundations of resting-state and task-based functional connectivity in
577 the human brain. *Proc Natl Acad Sci U S A* 110(15):6169–6174.

578 [64] Hermundstad AM et al. (2014) Structurally-constrained relationships between cognitive states in the human
579 brain. *PLoS Comput Biol* 10(5):e1003591.

580 [65] Shen K, Hutchison RM, Bezgin G, Everling S, McIntosh AR (2015) Network structure shapes spontaneous
581 functional connectivity dynamics. *J Neurosci* 35(14):5579–5588.

582 [66] Richiardi J et al. (2015) Correlated gene expression supports synchronous activity in brain networks. *Science*
583 348(6240):1241–1244.

584 [67] Andellini M, Cannata V, Gazzellini S, Bernardi B, Napolitano A (2015) Test-retest reliability of graph metrics
585 of resting state MRI functional brain networks: A review. *J Neurosci Methods* 253:183–192.

586 [68] Deuker L et al. (2009) Reproducibility of graph metrics of human brain functional networks. *Neuroimage*
587 47(4):1460–1468.

588 [69] Hutchison RM et al. (2013) Dynamic functional connectivity: promise, issues, and interpretations. *Neuroimage*
589 80:360–378.

590 [70] Leonardi N, Shirer WR, Greicius MD, Van De Ville D (2014) Disentangling dynamic networks: Separated and
591 joint expressions of functional connectivity patterns in time. *Human brain mapping* 35(12):5984–5995.

592 [71] Barnes A, Bullmore ET, Suckling J (2009) Endogenous human brain dynamics recover slowly following cognitive
593 effort. *PLoS One* 4(8):e6626.

594 [72] Gerraty RT, Davidow JY, Wimmer GE, Kahn I, Shohamy D (2014) Transfer of learning relates to intrin-
595 sic connectivity between hippocampus, ventromedial prefrontal cortex, and large-scale networks. *J Neurosci*
596 34(34):11297–11303.

597 [73] Albert NB, Robertson EM, Miall RC (2009) The resting human brain and motor learning. *Current Biology*
598 19(12):1023–1027.

599 [74] Taren AA et al. (2015) Mindfulness meditation training alters stress-related amygdala resting state functional
600 connectivity: a randomized controlled trial. *Social cognitive and affective neuroscience* p. nsv066.

601 [75] Pievani M, de Haan W, Wu T, Seeley WW, Frisoni GB (2011) Functional network disruption in the degenerative
602 dementias. *Lancet Neurol* 10(9):829–843.

603 [76] Betzel RF et al. (2014) Changes in structural and functional connectivity among resting-state networks across
604 the human lifespan. *Neuroimage* 102(Pt 2):345–357.

605 [77] Eilam-Stock T et al. (2014) Abnormal autonomic and associated brain activities during rest in autism spectrum
606 disorder. *Brain* 137(Pt 1):153–171.

607 [78] Dumontheil I (2014) Development of abstract thinking during childhood and adolescence: The role of rostrolat-
608 eral prefrontal cortex. *Developmental cognitive neuroscience* 10:57–76.

609 [79] Dixon ML, Christoff K (2014) The lateral prefrontal cortex and complex value-based learning and decision
610 making. *Neuroscience & Biobehavioral Reviews* 45:9–18.

611 [80] Fodor JA (1983) *Modularity of Mind: An Essay on Faculty Psychology.* (MIT Press).

612 [81] Newman MEJ (2006) Modularity and community structure in networks. *Proceedings of the National Academy*
613 *of Sciences U S A* 103(23):8577–8696.

614 [82] Grent-'t Jong T, Oostenveld R, Jensen O, Medendorp WP, Praamstra P (2014) Competitive interactions in
615 sensorimotor cortex: oscillations express separation between alternative movement targets. *J Neurophysiol*
616 112(2):224–232.

617 [83] Luber B, Lisanby SH (2014) Enhancement of human cognitive performance using transcranial magnetic stimu-
618 lation (TMS). *Neuroimage* 85(Pt 3):961–970.

619 [84] Enriquez-Geppert S, Huster RJ, Herrmann CS (2013) Boosting brain functions: Improving executive functions
620 with behavioral training, neurostimulation, and neurofeedback. *Int J Psychophysiol* 88(1):1–16.

621 [85] Brainard DH (1997) The psychophysics toolbox. *Spatial vision* 10:433–436.

622 [86] Schmidt RA, Lee T (1988) *Motor control and learning.* (Human kinetics).

623 [87] Rosenbaum DA (2009) *Human motor control.* (Academic press).

624 [88] Snoddy GS (1926) Learning and stability: a psychophysiological analysis of a case of motor learning with clinical
625 applications. *Journal of Applied Psychology* 10(1):1.

626 [89] Crossman E (1959) A theory of the acquisition of speed-skill. *Ergonomics* 2(2):153–166.

627 [90] Newell A, Rosenbloom PS (1981) Mechanisms of skill acquisition and the law of practice. *Cognitive skills and*
628 *their acquisition* 1.

629 [91] Heathcote A, Brown S, Mewhort D (2000) The power law repealed: The case for an exponential law of practice.
630 *Psychonomic bulletin & review* 7(2):185–207.

631 [92] Dale AM, Fischl B, Sereno MI (1999) Cortical surface-based analysis: I. segmentation and surface reconstruction.
632 *Neuroimage* 9(2):179–194.

633 [93] Cox RW (1996) Afni: software for analysis and visualization of functional magnetic resonance neuroimages.
634 *Computers and Biomedical research* 29(3):162–173.

635 [94] Greve DN, Fischl B (2009) Accurate and robust brain image alignment using boundary-based registration.
636 *Neuroimage* 48(1):63–72.

637 [95] Smith SM et al. (2004) Advances in functional and structural mr image analysis and implementation as fsl.
638 *Neuroimage* 23:S208–S219.

639 [96] Whitfield-Gabrieli S (2009) Artifact detection tools.

640 [97] Behzadi Y, Restom K, Liau J, Liu TT (2007) A component based noise correction method (compcor) for bold
641 and perfusion based fmri. *Neuroimage* 37(1):90–101.

642 [98] Murphy K, Birn RM, Handwerker DA, Jones TB, Bandettini PA (2009) The impact of global signal regression
643 on resting state correlations: are anti-correlated networks introduced? *Neuroimage* 44(3):893–905.

644 [99] Saad ZS et al. (2012) Trouble at rest: how correlation patterns and group differences become distorted after
645 global signal regression. *Brain connectivity* 2(1):25–32.

646 [100] Chai XJ, Castañón AN, Öngür D, Whitfield-Gabrieli S (2012) Anticorrelations in resting state networks without
647 global signal regression. *Neuroimage* 59(2):1420–1428.

648 [101] Wang J et al. (2009) Parcellation-dependent small-world brain functional networks: A resting-state fmri study.
649 *Human brain mapping* 30(5):1511–1523.

650 [102] Wig GS, Schlaggar BL, Petersen SE (2011) Concepts and principles in the analysis of brain networks. *Annals*
651 *of the New York Academy of Sciences* 1224(1):126–146.

652 [103] Woolrich MW et al. (2009) Bayesian analysis of neuroimaging data in fsl. *Neuroimage* 45(1):S173–S186.

653 [104] Lund TE, Hanson LG (2001) Physiological noise reduction in fmri using vessel time-series as covariates in a
654 general linear model. *Neuroimage* 13(6):191.

655 [105] Newman ME (2006) Modularity and community structure in networks. *Proceedings of the National Academy of*
656 *Sciences* 103(23):8577–8582.

# Supporting Information

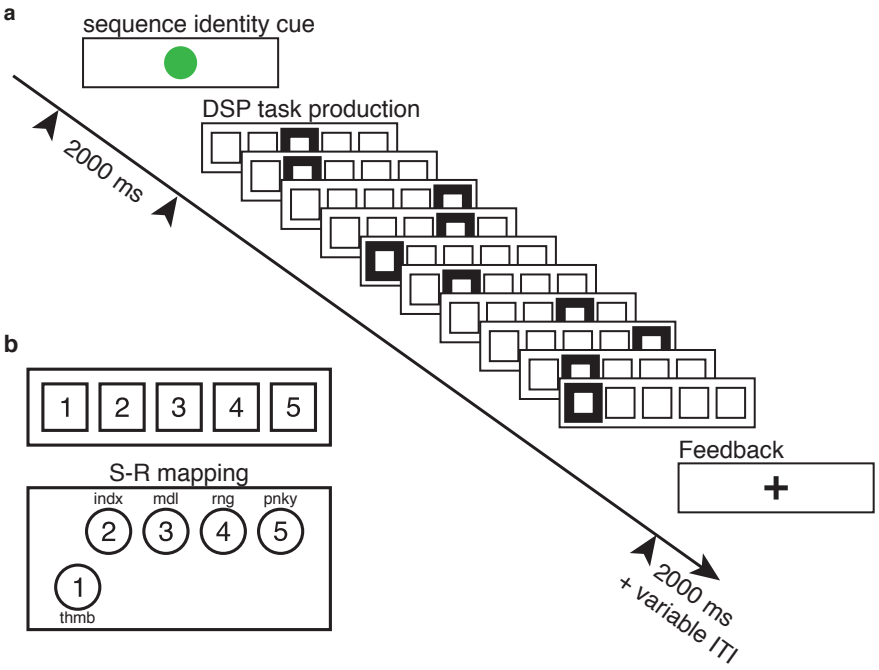


Figure S1: **Trial structure and stimulus-response mapping.**
(a) Each trial began with the presentation of a sequence-identity cue that remained on screen for 2 seconds. Each of the six trained sequences was paired with a unique identity cue. A discrete sequence-production (DSP) event structure was used to guide sequence production. The onset of the initial DSP stimulus (thick square, colored red in the task) served as the imperative to produce the sequence. A correct key press led to the immediate presentation of the next DSP stimulus (and so on) until the ten-element sequence was correctly executed. Participants received a + as feedback to signal that a sequence was completed and to wait (approximately 0–6 s) for the start of the next trial. This waiting period was called the intertrial interval (ITI). At any point, if an incorrect key was hit, a participant would receive an error signal (not shown in the figure), and the DSP sequence would pause until the correct response was received.
(b) There was direct stimulus-response mapping between a conventional keyboard or an MRI-compatible button box (lower left) and a participants right hand, so that the leftmost DSP stimulus cued the thumb and the rightmost stimulus cued the pinky finger. Note that the button location for the thumb was positioned to the lower left for maximum comfort and ease of motion.

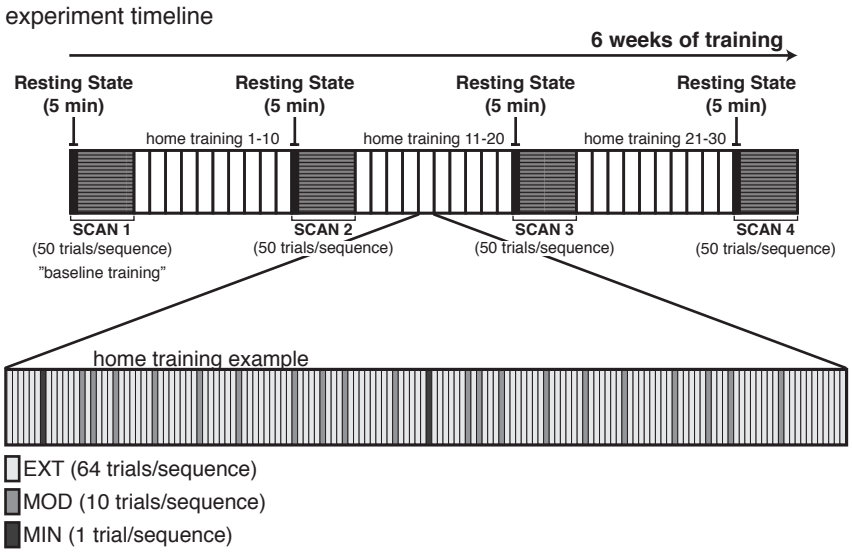


Figure S2: **Experiment protocol and timeline.**
(a) The experiment protocol comprised of six weeks of training of six distinct motor sequences. Following a brief explanation of the task instructions, a initial MRI scan session was held during which blood oxygen level-dependent (BOLD) signals were acquired from each participant. The scan session began with a resting state scan lasting 5 minutes where participants were instructed to remain awake and with eyes open without fixation. During the remainder of the first scan session (baseline training), participants practiced each of six distinct motor sequences for 50 trials each, or approximately 1.5 hour. They were then instructed to continue practicing the motor sequences at home using a trainind module that was installed by the experimenter (N.F.W.) on their personal laptops. Participants completed a minimum of 30 home training sessions, which were interleaved with two additional scan sessions, each occurring after at least 10 home training sessions. A final scan session was held following the completion of the 6 weeks of training. The same protocol was followed in each of the four scan sessions: a 5 minute resting state scan, followed by approximately 1.5 hour of the DSP task, where each of six distinct motor sequences was practiced for 50 trials each. (b) Most of the motor sequence training occurred at home, between scanning sessions. An ideal home training session consisted of 150 trials with sequences practiced in random order (randomization used the Mersenne Twister algorithm of Nishimura and Matsumoto as implemented in the random-number generator rand.m of MATLAB version 7.1). Each EXT sequence was practiced for 64 trials, each MOD sequence was practiced for 10 trials, and each MIN sequence was practiced for 1 trial.

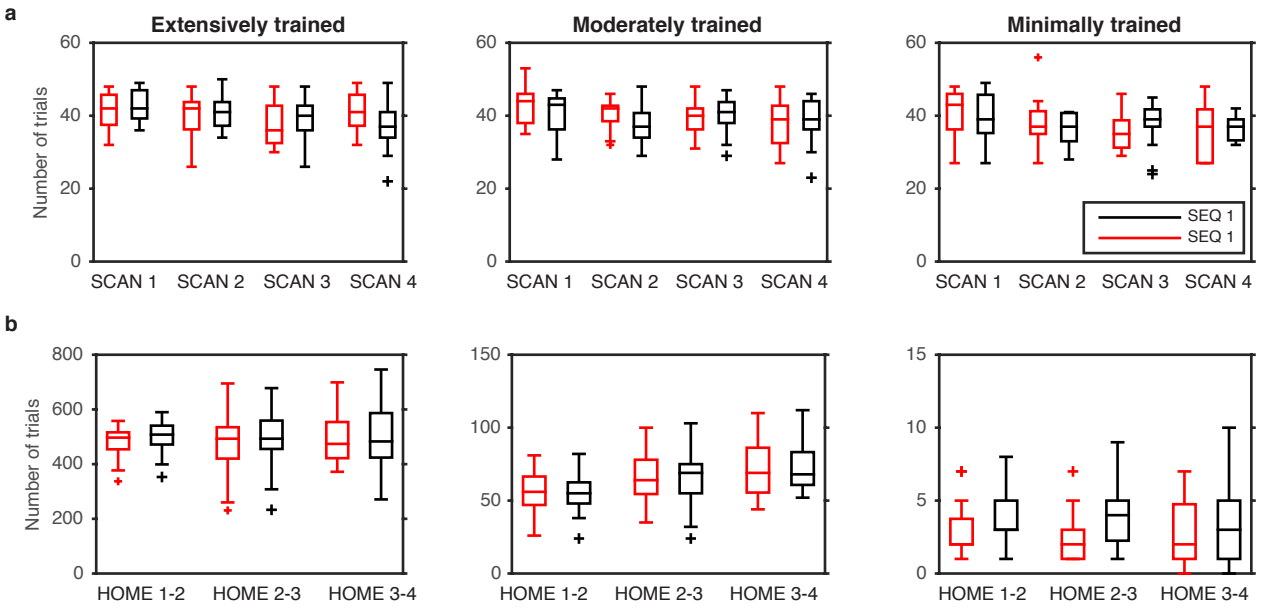


Figure S3: **Number of error-free trials performed per session.**
(a) Number of trials practiced in each scan session. *Left panel:* Extensive training (EXT) session; *Middle panel:* Moderate training (MOD) session; *Right panel:* Minimal training (MIN) session. Box plot represents quartiles and + symbols represent outliers. The variability in the number of executed trials during scan sessions arose mainly from software or hardware difficulties.
(b) Number of trials practiced in each home session. *Left panel:* Extensive training (EXT) session; *Middle panel:* Moderate training (MOD) session; *Right panel:* Minimal training (MIN) session. Box plot represents quartiles and + symbols represent outliers. The variability in the number of executed trials are due to some subjects training more days than others between successive scanning sessions.

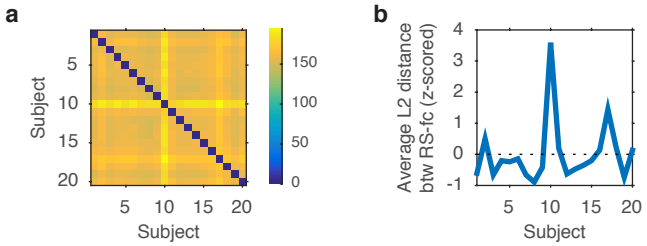


Figure S4: **Subject exclusion criterion.**
(a) We aimed to identify corrupted resting-state data by sleep or poor data quality by tracking functional connectivity outliers from our group norm. We calculated the average L2 distance between corresponding cells of the 626x626 functional connectivity matrices from all pairs of participants, summarized in the dissimilarity matrix of the figure.
(b) Average L2 distance between the RS-fc matrix of one participant and that from all others. With the exception of subject 10, all subjects were within 1.5 standard deviations from each other. The resting state data from subject 10 differed on average by 3.6 standard deviations from the others and, therefore, was excluded from the remainder of the analyses.

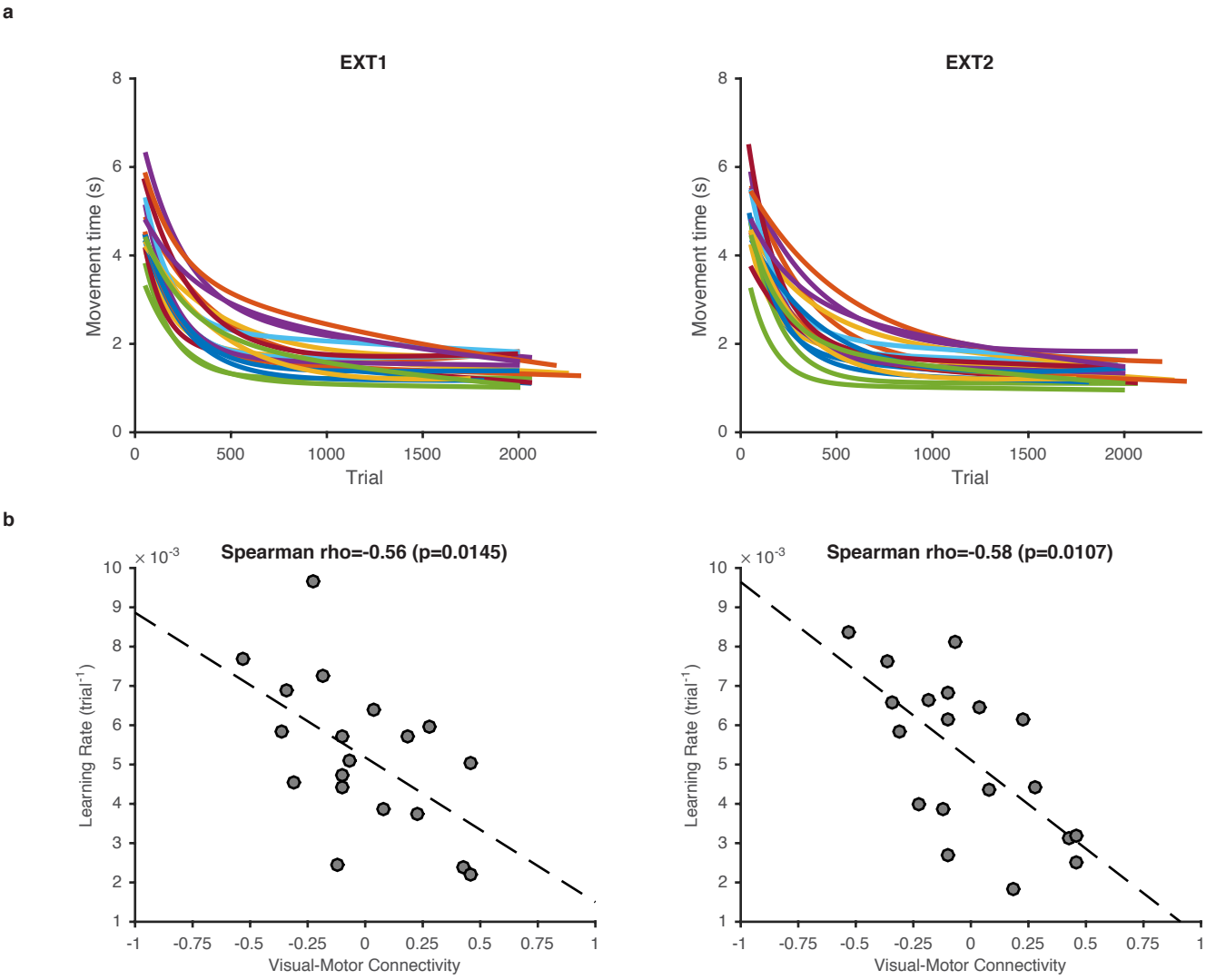


Figure S5: **Learning curves from individual participants.**
(a) Time required to execute a complete motor sequence (Movement Time), as a function of trial number. Colored curves are two-term exponential fits of the movement times from each participant. Learning happened for all participants, as evidenced by the reduction of movement times, but with large variability in the decay rates. Left and right panels correspond to the two extensively trained sequences.
(b) Functional connectivity between visual and somato-motor regions estimated at rest reliably predicts individual differences in learning rate for both EXT1 (left panel) and EXT2 (right panel) sequences.

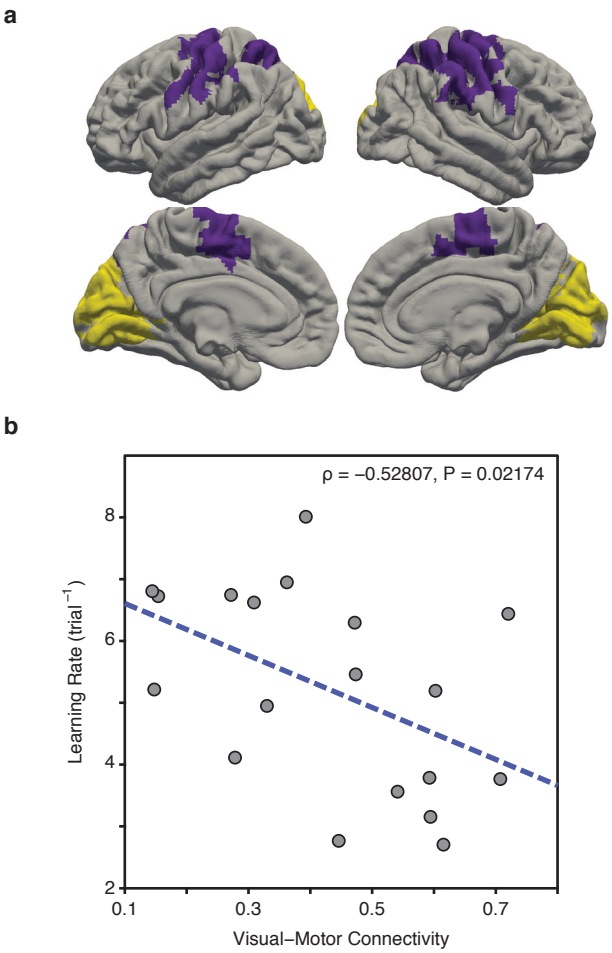


Figure S6: **Replication of Fig. 2 with uncentered functional connectivity values**
(a) Same as Fig. 2a: Visual (yellow) and somato-motor (purple) modules.
(b) Similar to Fig. 2b. The removal of various signal components present throughout most of the brain (in particular by the tCompCor method) leads to a shift on the distribution of functional connectivity values, giving rise to negative correlations (Fig. 2b). Here, we use a less stringent noise removal pipeline (same as original but without the tCompCor method) that does not shift the range of correlation values. Similarly to our original results, we observe that functional connectivity between visual and somato-motor modules, estimated at rest and prior to learning, reliably predicts individual differences in future learning rate ($\rho = -0.5280, P = 0.02174$). The weaker statistical relationship is likely a consequence of residual physiological noise [104].

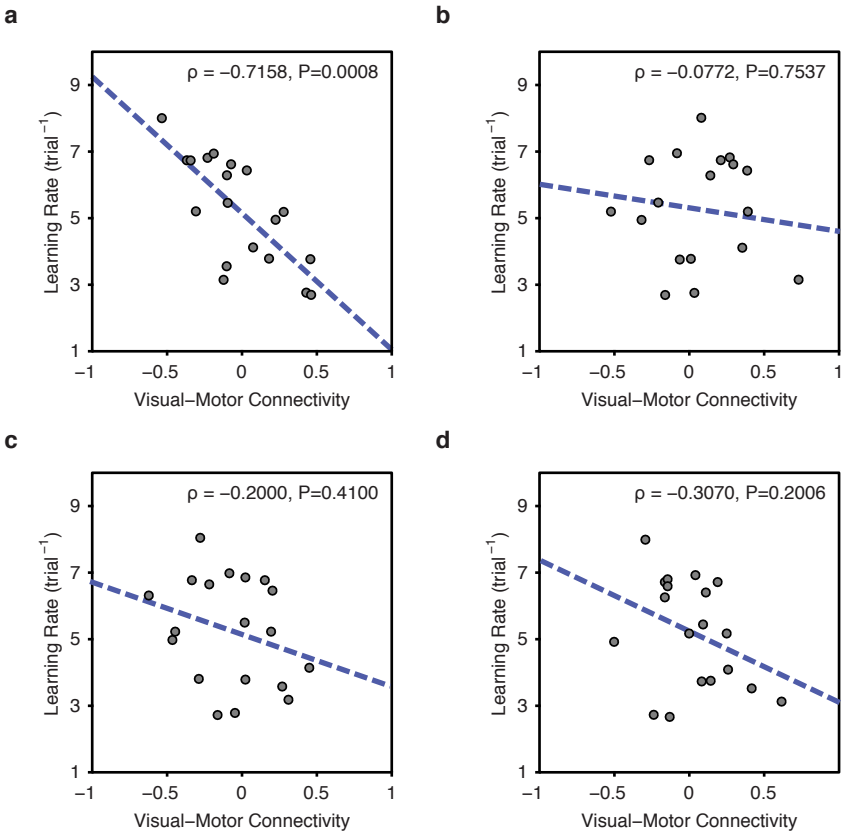


Figure S7: **Correlation between visual-motor connectivity at various sessions and overall learning rate.** (a) Relationship between visual-motor connectivity estimated from the resting-state scan acquired in SESSION 1 and overall learning rate. The Spearman correlation between these two quantities is $\rho = -0.7158, P = 0.0008$.
(b) Relationship between visual-motor connectivity estimated from the resting-state scan acquired in SESSION 2 and overall learning rate. The Spearman correlation between these two quantities is $\rho = -0.0772, P = 0.7537$.
(c) Relationship between visual-motor connectivity estimated from the resting-state scan acquired in SESSION 3 and overall learning rate. The Spearman correlation between these two quantities is $\rho = -0.2000, P = 0.4100$.
(d) Relationship between visual-motor connectivity estimated from the resting-state scan acquired in SESSION 4 and overall learning rate. The Spearman correlation between these two quantities is $\rho = -0.3070, P = 0.2006$. The combined p-value across all four tests, calculated with Fisher's method, is $P = 0.0112$.

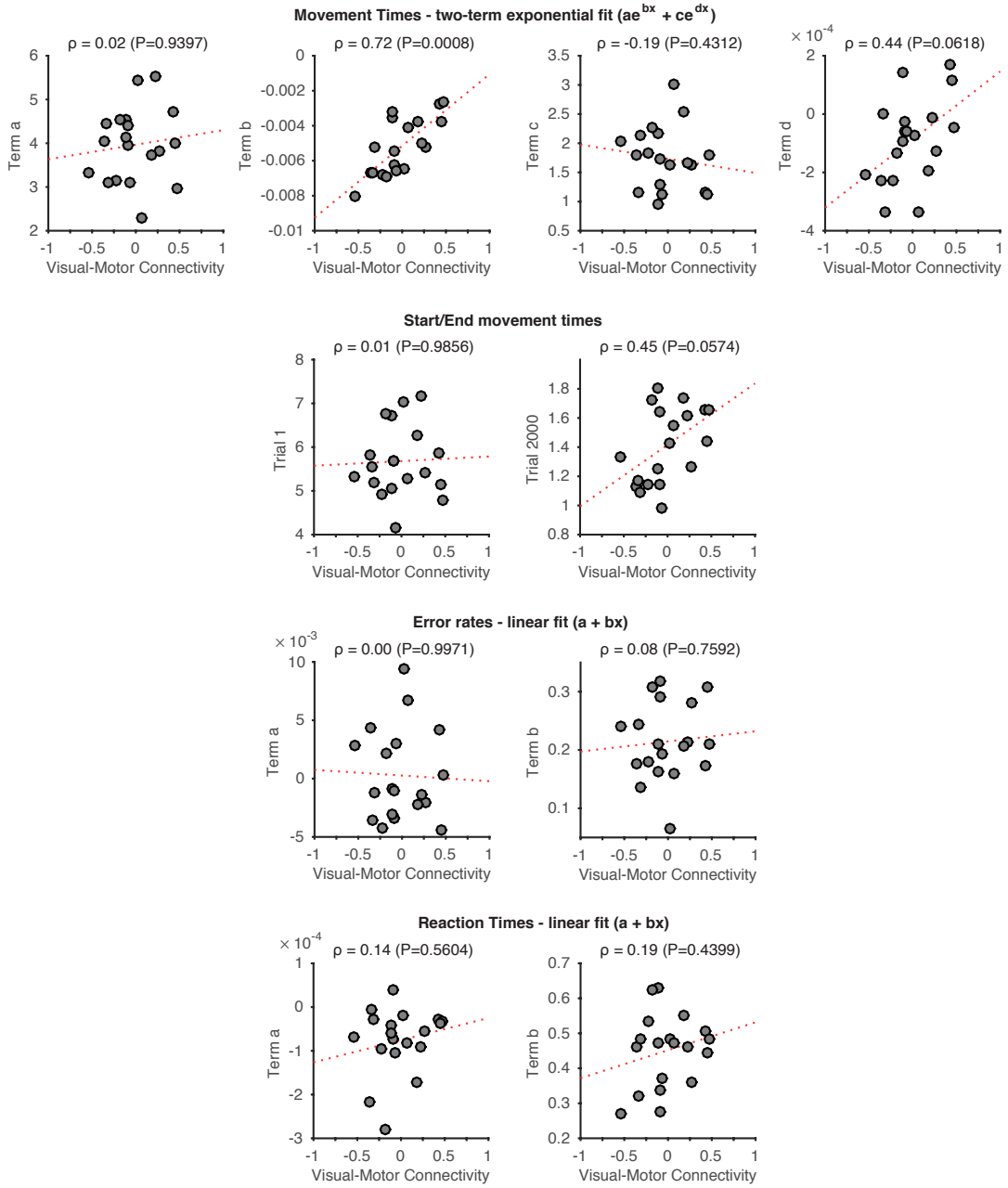


Figure S8: **Statistical relationship between resting visual-motor connectivity and different behavioral markers.**
(a) Relationship between resting-state visual-motor connectivity estimated from the resting-state scan acquired in SESSION 1 and each of the four parameters from the two-term exponential fits of the movement times. Notice the marginal significance of the correlation between visual-motor connectivity and *term d*, suggesting that visual-motor connectivity correlates not only with the faster drop-off parameter (*term b*), but also with the slower decay parameter (*term d*).
(b) Relationship between resting-state visual-motor connectivity estimated from the resting-state scan acquired in SESSION 1 and the fitted start movement time (*left*); similarly for fitted end movement time (*right*). Notice the marginal significance of the correlation between visual-motor connectivity and movement time at trial 2000, suggesting that participants with high visual-motor connectivity tend to have longer movement times.
(c) Relationship between resting-state visual-motor connectivity estimated from the resting-state scan acquired in SESSION 1 and both parameters from a linear fit to the error rates.
(d) Relationship between resting-state visual-motor connectivity estimated from the resting-state scan acquired in SESSION 1 and both parameters from a linear fit to the reaction times.

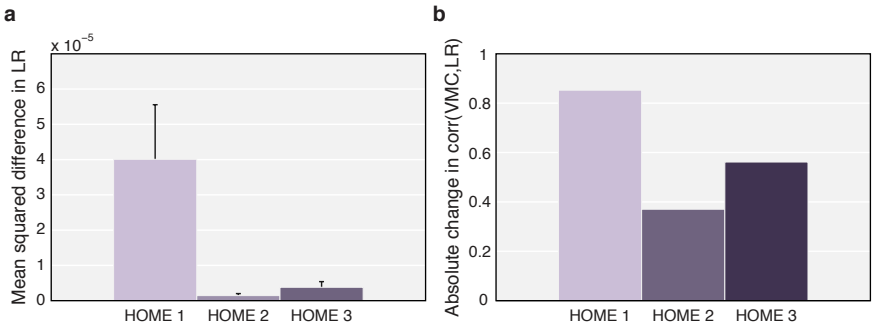


Figure S9: **Effect of removing trials from different portions of the learning curve.**
(a) Effect of removing trials from different epochs of training on the estimated learning rates. Removing HOME 1 trials, corresponding to home training sessions between the first and second scan sessions, had the largest impact on the estimations of learning rate using a two-term exponential fit.
(b) Effect of removing trials from different epochs of training on the correlations between visual-motor connectivity and learning rates. Removing HOME 1 trials also had the largest absolute impact on the Spearman's correlations coefficients.

# Acknowledgements

DSB acknowledges support from the John D. and Catherine T. MacArthur Foundation, the Alfred P. Sloan Foundation, the Army Research Laboratory through contract no. W911NF-10- 2-0022 from the U.S. Army Research Office, the Army Research Office through contract no. W911NF-14-1-0679, the Office of Naval Research Young Investigator Program, the NIH through award R01-HD086888 and 1R01HD086888-01, and the National Science Foundation awards #BCS-1441502, #BCS-1430087, and #PHY-1554488. The content is solely the responsibility of the authors and does not necessarily represent the official views of any of the funding agencies.


# Author Contributions

NW and SG developed the experimental paradigm. NW collected the data. DB, MM designed the research. MM analyzed the data. MM, NW, AB, GA, and DB wrote the paper.


# Keywords

fMRI; functional connectivity; network science; cognitive systems; brain networks; behavioral adaptability; human learning